Chapter 3. High-Frequency (>100 GHz) and High-Speed (<1 ps) Electronic Devices

Academic and Research Staff

Professor Qing Hu

Visiting Scientists and Research Affiliates

Dr. Thomas Schäpers, Dr. Simon Verghese

Graduate Students

James Ernstmeyer, Rajesh K. Gupta, Brian R. Jacobson, Jurgen H. Smet, Rolf A. Wyss

Undergraduate Students

David K. Chow, Elliot E. Hui

Technical and Support Staff

Barbara A. King

3.1 Facility for Millimeter-wave and THz Frequencies

Professor Hu's laboratory is equipped with various millimeter-wave and infrared sources which can generate coherent and incoherent radiation up to 30 THz. These include: Gunn oscillators at W-band frequencies (75-110 GHz); a frequency doubler, tripler, and quadrupler using Schottky diodes at 200, 300, and 400 GHz; an optically pumped far-infrared laser which generates coherent radiation up to 8 THz; and an infrared Fourier transform spectrometer which is capable of performing linear spectroscopy from 45 GHz to 30 THz and beyond. This laboratory is also equipped with various cryogenic millimeter-wave and infrared detectors. These include: Si composite bolometers, InSb hot-electron bolometers, superconductor-insulator-superconductor (SIS) receivers, and high-Tc Josephson detectors. There are many infrared cryostats which can cool the devices from 0.3 K to 77 K.

3.2 Far-infrared Studies of Antenna-coupled Quantum-effect Devices

Sponsor

MIT Research Laboratory of Electronics
Postdoctoral Fellowship
National Science Foundation
Grant DMR 90-22933

Project Staff

Rolf A. Wyss, Dr. Thomas Schäpers, Professor Qing Hu, in collaboration with Professor Jesús A. del Alamo and Jülich GmbH Company[1]

Quantum transport has been one of the most active fields in solid-state physics in recent years. Advances in material preparation have made quantum phenomena profound in electron transport for many semiconductor quantum devices such as quantum point contacts, quantum dots, quantum wires, quantum wells, superlattices, etc. In clean samples and at low temperatures, electrons can travel through the whole sample without suffering phase-destructive scattering. Extensive work has been done to study various features of such phase-coherent quantum transport. However, the experiments reported so far are limited to measurements by dc transport and far-infrared spectroscopy.

[1] Jülich, Germany.

It is well known in the field of superconducting tunneling that photons can assist the tunneling process, provided that the tunneling is elastic. In a broad sense, elastic tunneling is a phase-coherent quantum transport process in a classically forbidden region. Therefore, all the results of photon-assisted tunneling can be applied to the study of photon-assisted quantum transport in semiconductor devices. This will provide a new dimension to study the exciting quantum transport phenomena. Novel long-wavelength optoelectronic devices may also emerge from this research.

In this project, we study the interaction between far-infrared photons and ballistic electrons in quantum point contact devices, whose schematic is shown in figure 1a.

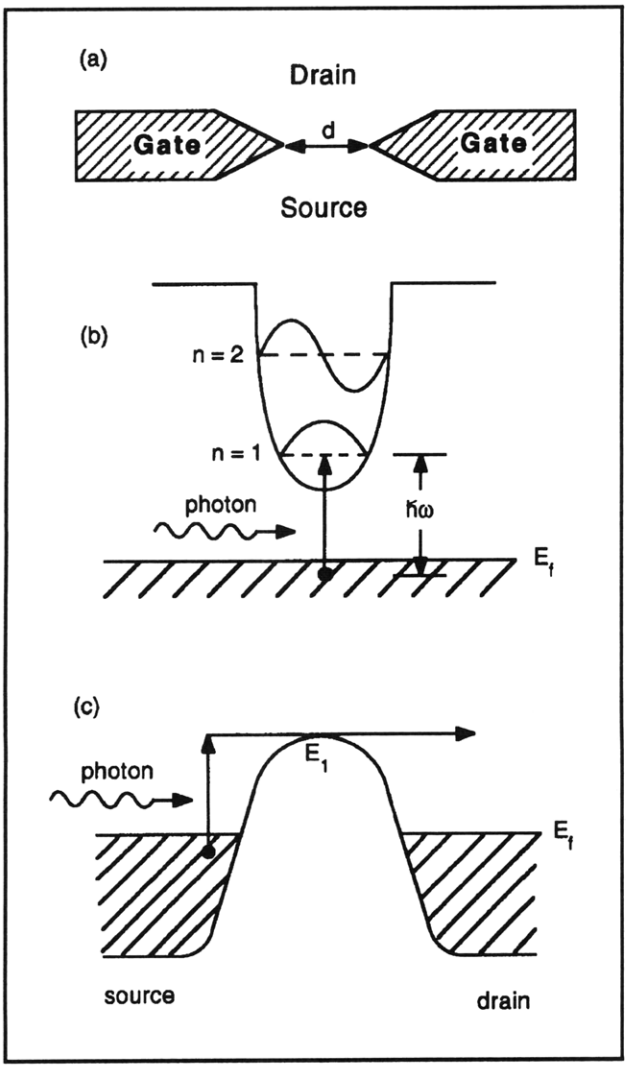

Figure 1. (a) Schematic of a quantum point contact. (b) and (c) Illustration of photon-assisted over-the-barrier quantum transport.

We have fabricated several antenna-coupled quantum point contact devices using a combination of optical and electron-beam lithography. Figure 2 shows the SEM photographs of one of the devices. The split-gate electrodes (the vertical leads) also serve as the terminals of a log-periodic antenna, whose function is to couple the far-infrared radiation of millimeter wavelength to the point contact of submicron dimensions.

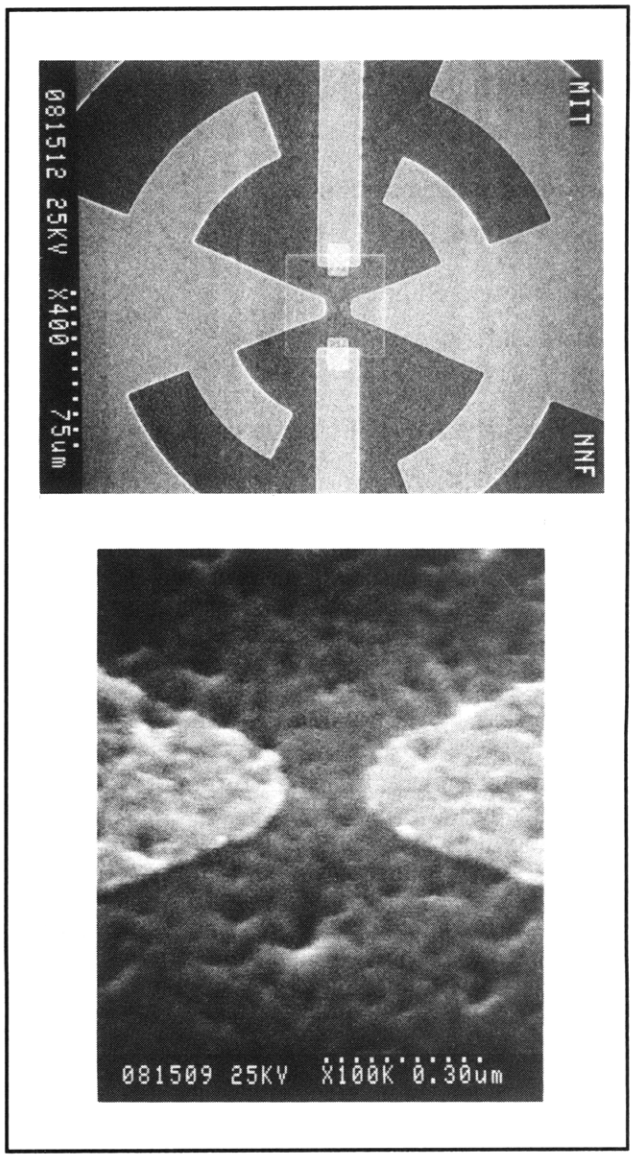

Figure 2. (a) SEM (with a magnification of 400) of a quantum point contact with a log-periodic antenna. (b) Central region of the quantum point contact. The opening of the split-gate electrodes is 0.15 μm.

The dc transport measurement of the drain/source transport showed fifteen quantized conductance steps, indicating the high quality of the devices. Under coherent far-infrared radiation at 285 GHz, a

pronounced photon-induced drain/source current is produced throughout a gate voltage range in which the device exhibits the behavior of a one-dimensional electron system. This photon-induced current is attributed to a bolometric effect as described in the previous report.

In addition to the photoconductive effect, we have recently discovered a pronounced photovoltaic effect in several antenna-coupled quantum point contacts irradiated from 280 GHz to 2.5 THz. Figure 3a shows the drain/source current of an irradiated quantum point contact without external drain/source bias. This induced current tracks the subband structure in a very regular manner that is similar to the transconductance of the device measured without radiation. We have identified this photovoltaic effect as a result of thermopower due to an asymmetric heating of the source and drain. This analysis is supported by experimental evidence that, by shifting the focal spot of the radiation, we can reverse the polarity of the photon-induced current, as shown in figure 3b. This is a direct observation of thermopower in a one-dimensional electron system. We are currently fitting the measured photon-induced current with quantum transport theories by taking the finite drain/source thermal conductance into account and by using a nonlinear gate voltage versus Fermi energy relation.

To maximize the photon-assisted quantum process, we have recently started investigating the possibility of photon-excited bound-to-extended-state transition in an antenna-coupled lateral quantum-well device (or PRESTFET), as shown in figure 4. In this device, the dipole-transition matrix element is on the order of the well width, which is much greater than that in a quantum-point-contact device. Furthermore, the drain/source resistance of a lateral QW device is on the order 100 Ω, which is much smaller than that of a quantum point contact, making impedance matching with the planar antennas much easier. Vertical quantum-well versions of this device have been well developed for detection applications around 10-μm wavelength region, and video cameras with 128 × 128 pixels have been made with temperature sensitivities around 10 mK.

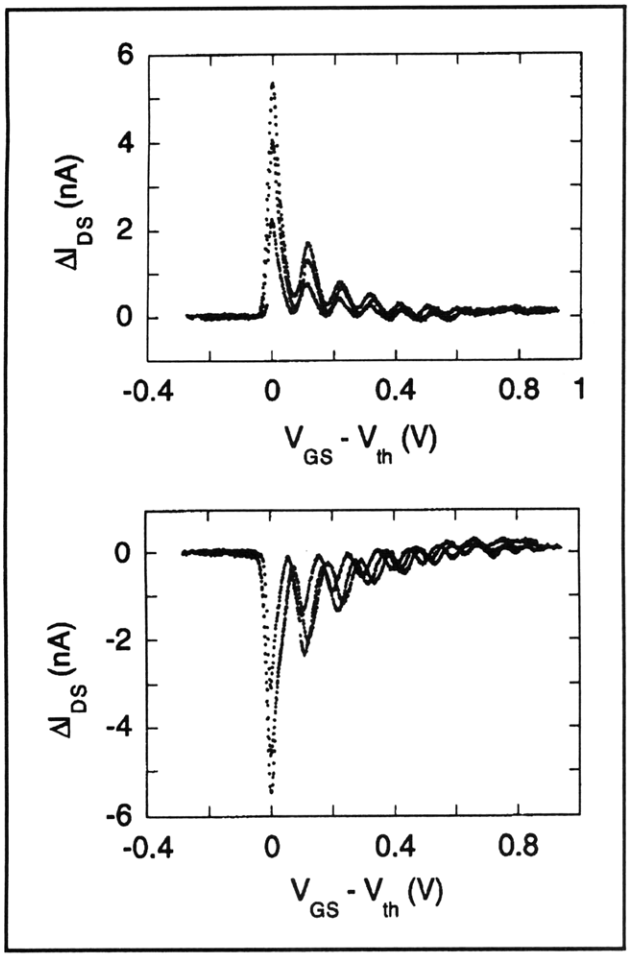

Figure 3. (a) Drain/source current of an antenna-coupled quantum point contact irradiated at different power levels at 280 GHz with zero external drain/source bias voltage. (b) Same as (a), except the far-infrared radiation spot is shifted.

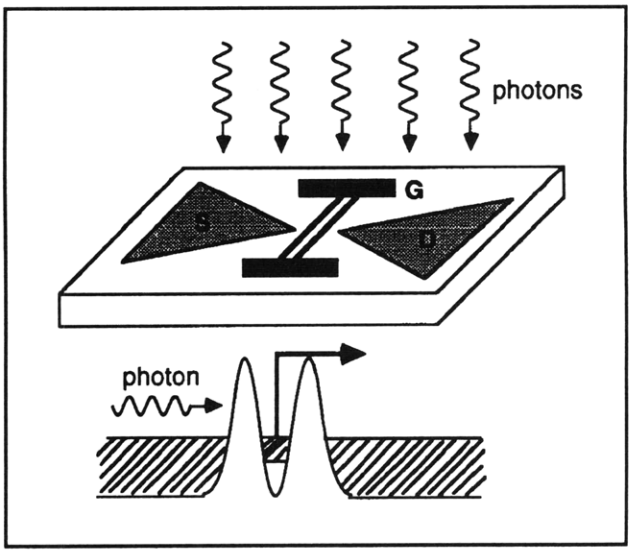

Figure 4. (a) Schematic of an antenna-coupled lateral quantum-well device irradiated at far-infrared frequencies. (b) Illustration of photon-excited bound-to-extended-state transition in these devices. Clearly, the operating frequencies of these devices can be tuned electrically by changing the barrier heights.

3.3 Femtosecond Dynamical Studies of Quantum Devices for Ultrafast Electronic Applications

Sponsor

MIT Lincoln Laboratory
Advanced Concept Program

Project Staff

Dr. Simon Verghese, Professor Qing Hu, in collaboration with Dr. Elliot Brown[2]

Solid-state physics and electrical engineering communities are witnessing a trend in which electronic devices are becoming smaller and their speeds are becoming faster. This trend is driven by modern society's insatiable appetite for increasing capacity for information processing and transmission. As a result, the size of the smallest features of state-of-the-art devices has decreased to just several hundred angstroms. At this length scale, intersubband spacing and Coulomb interaction energy are comparable to the Fermi energy, and consequently the devices behave as quantum mechanical systems (or artificial atoms). In a related project (see section 3.2), we have studied transport properties of antenna-coupled quantum point contacts under coherent far-infrared radiation whose frequencies are comparable to the intersubband spacing in the point contact. In this ACC project, we will carry out transport studies in time domain by using subpicosecond electrical pulses generated by Auston switches to study the dynamical processes of electrons in quantum-effect structures. This work will substantially enhance our understanding of the dynamics of quantum structures, and novel ultrafast devices may also emerge from this research.

Our past work in frequency domain has yielded new information about quantum point contact devices (such as radiation-induced current and thermopower), and we intend to continue that effort to improve the device parameters (mainly to use better antenna structures to minimize heating and maximize the quantum process). A better approach would be to study the response of the quantum devices in time-resolved fashion by using a pump-and-probe method with a pulsed laser. A 100-fs laser pulse contains frequency components up to 10 THz, which should enable us to perform spectroscopic studies on quantum devices over a broad frequency range that covers all the interesting energy levels, namely the intersubband transition and Coulomb interaction energies. Furthermore, unlike a conventional far-infrared Fourier transform spectrometer, the brightness of a pulsed laser source will enable us to perform nonlinear spectroscopy. In addition, the short duration of the laser pulses minimizes heating effect and enhances quantum mechanical processes. Finally (and perhaps their most attractive feature), time-resolved studies can reveal information such as the time scale of transport process in quantum devices. One of the basic issues in determining the potential applications of quantum devices, this method may eventually answer some fundamental questions such as the traversal time of tunnel, which have intrigued physicists since the initial discovery of quantum mechanics.

We will pursue two types of measurements in this project. The first one involves a far-infrared spectrometer pumped by a mode-locked Ti:Sapphire laser which we have constructed recently, as shown in figure 5. In this set up, two antenna-coupled Auston switches are pumped by a $Ti:Al_2O_3$ pulsed laser. The THz electrical pulses are launched into free space and then combined by a beam splitter. The combined beam is a superposition of two coherent subpicosecond electrical pulses whose relative time delay can be varied. These combined pulses will then be focused onto an antenna-coupled quantum device to generate a dc electrical current in the device through the photon-assisted transport/tunneling process. The generated electrical current is proportional to the time autocorrelation function of the whole system, whose Fourier transform will give the frequency response of the system. This measurement is essentially the same as that made with a conventional far-infrared Fourier transform spectrometer (FTS), which uses a Hg-arc lamp as its source. There are some major advantages of the pulsed laser system, however. First, its source is much brighter than that of the FTS so that far-infrared nonlinear spectroscopy can be performed. Second, the short duration of the laser pulses minimizes the heating effect and thus enhances the relative strength of the photon-assisted quantum process.

---

[2] MIT Lincoln Laboratory, Lexington, Massachusetts.

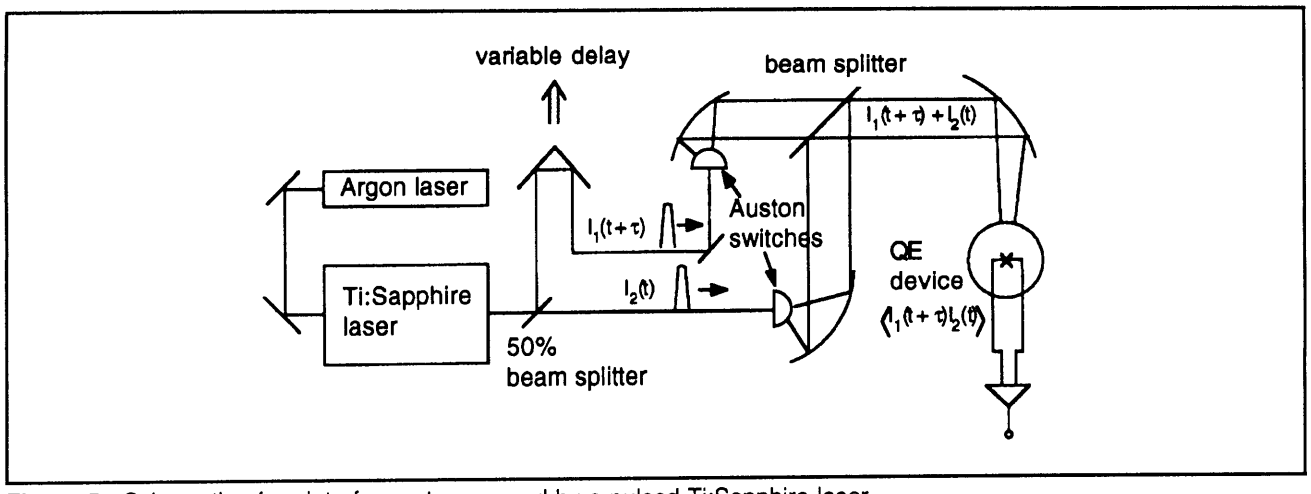

Figure 5. Schematic of an interferometer pumped by a pulsed Ti:Sapphire laser.

The second type of experiment involves a pump-and-probe method, by integrating two Auston switches *monolithically* with the quantum-effect (or Josephson) devices, as shown in figure 6. One switch will be used to apply a short electric pulse on the input, and the second one will be used to probe the output electrical current in a time-resolved fashion. This scheme differs from the first one in that the pump and probe beams are focused on *different* spots. In this way, we can measure the time scale of the transport process from the input to the output, as well as the spectroscopic information of the system. To achieve a high speed from the Auston switches, lattice-matched low-temperature-grown (LTG) GaAs materials which have subpicosecond recombination time will be used.

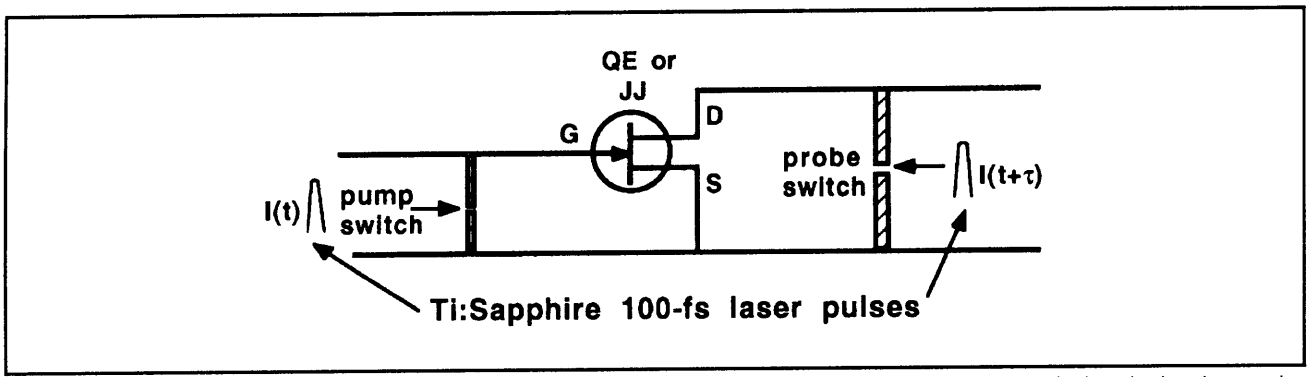

Figure 6. Schematic of a three-terminal (QE or Josephson) device pumped by a subpicosecond electrical pulse at the input, and the induced output current can be time-resolved by another time-delayed probe beam.

3.4 High-T_c Superconducting Josephson Devices

Sponsor

Advanced Research Projects Agency
Contract MDA972-90-C-0021

Project Staff

Rajesh K. Gupta, Professor Qing Hu, in collaboration with Twente University

Many superconducting analog devices have been demonstrated to have higher sensitivities, higher speed and frequency limit, and lower power dissipation than competing semiconductor devices. Among them, the most successful ones are superconducting quantum interference devices (SQUIDs) and millimeter-wave detectors.

The discovery of superconductors with their superconducting transition temperature higher than liquid nitrogen temperature (high T_c superconductors) has opened up new and exciting possibilities in electronic device technology. High-temperature versions of the superconducting devices mentioned above will find a much wider-range application wherever refrigeration is a problem. The key element of all superconducting analog and digital devices is the Josephson junction. This junction is formed by two superconductors weakly coupled together electrically. The supercurrent flowing

through the Josephson junction oscillates at the Josephson frequency f = 2 eV/h (500 GHz/mV), when a voltage is applied across the junction. Most of the useful applications of Josephson devices, such as high-frequency and high-speed signal processors and high-sensitivity SQUID magnetometers whose high precision results from averaging over many cycles of the Josephson oscillations, result from this high-frequency oscillation.

In collaboration with the Dutch group headed by Professor Horst Rogalla,[3] which is the leading group in fabricating high-quality high-Tc Josephson junctions, we have studied the response of a YBCO/PBCO/YBCO ramp-type junction to coherent radiation at 176 GHz and 270 GHz. The I-V characteristic of the junction closely resembles the prediction of the RSJ model (resistively-shunted-junction). The critical current and the normal resistance product I_cR_n of the junction is 0.25 mV at 5 K. The millimeter-wave radiation is coupled to the junction via a quasioptical structure that focuses the radiation onto the junction through a yttrium-stabilized ZrO_2 substrate. At 176 GHz, we have observed as many as six Shapiro steps at the maximum power level of our Gunn Oscillator-pumped frequency doubler. This implies a Josephson oscillation up to 1 THz. Shapiro steps are still visible up to 65 K.

The amplitudes of the zeroth, first, and second Shapiro steps, as functions of the square root of the radiation power, agree remarkably well with a Bessel function fit. This Bessel-like behavior is an indication that the junction is voltage-biased at the radiation frequency. This is in great contrast with other experiments carried at lower frequencies, in which a current-biased behavior is usually observed. For a voltage-biased RSJ-like junction, the detector response can be predicted analytically. The current responsivity of our device, defined as the induced dc current per unit RF power, is calculated to be 2×10^3 A/W, which is comparable to the quantum efficiency $e/\hbar\omega \approx 1.4 \times 10^3$ A/W at this frequency.

Taking advantage of the ideal RSJ-like behavior of our high-Tc Josephson junctions, we have studied the noise effect on their millimeter-wave response by using Ambegaokar-Halperin-Lee (AHL) theory which is well established for low-Tc junctions. Such a study is crucial in developing high-sensitivity devices such as millimeter-wave receivers and SQUID amplifiers. According to AHL theory, noise effects on an RSJ junction behavior are exhibited by the rounding of the sharp corner transition from the constant voltage states near the critical current and the Shapiro steps to the "running states" that exhibit finite differential resistance. This rounding results from a dephasing of the Josephson pair current due to thermal activation. The susceptibility to noise is greatest in these transition regions. AHL theory predicts that the noise-rounded I-V curve near a Shapiro step is given by:

$$\delta V = \frac{\Delta I_n R_n}{2\gamma}\left(1 - e^{-2\pi\gamma\delta I_n/\Delta I_n}\right)\frac{1}{T_1}\left(1 + \beta_c \frac{T_2}{T_1}\right), \qquad (1)$$

where,

$$T_1 = \int_0^{\pi} I_0(\gamma \sin\theta) e^{-2\gamma\theta\delta I_n/\Delta I_n}\, d\theta, \qquad (2)$$

and

$$T_2 = \int_0^{\pi} \sin\theta I_1(\gamma \sin\theta) e^{-2\gamma\theta\delta I_n/\Delta I_n}\, d\theta. \qquad (3)$$

Here, δV is the actual voltage measured from the center of a given step number n, ΔI_n is the total amplitude of the noiseless current step, δIn is the current measured from the center of the nth step for $\delta I_n \leq \Delta I_n/2$, and R_n is the voltage-independent normal state resistance as found in the RSJ. The Stewart-McCumber parameter β_c is equal to $(e\Delta I_n C/\hbar)R_n^2$, and γ is equal to $\hbar\Delta I_n/2ek_BT_N$. Together they give a complete description of the noise in the system. Figures 7 and 8 show the comparison between the measured and calculated I-V curves near the zeroth, first, and second Shapiro steps. The noise response of the high-Tc Josephson junction can be analyzed extremely well with AHL theory.

In figure 9, we plot the noise temperature T_N, which is used as a parameter in fitting the AHL theoretical calculation to our measured I-V curves, as a function of the physical bath temperature T_p that is monitored independently by a Si thermometer. Over a broad temperature range from 10 K to 70 K, T_N is close to the physical bath temperature to within 10 percent, indicating that all high-Tc superconducting active devices based on Josephson effect could reach thermal-noise limited sensitivity.

[3] Twente University, Enschede, The Netherlands.

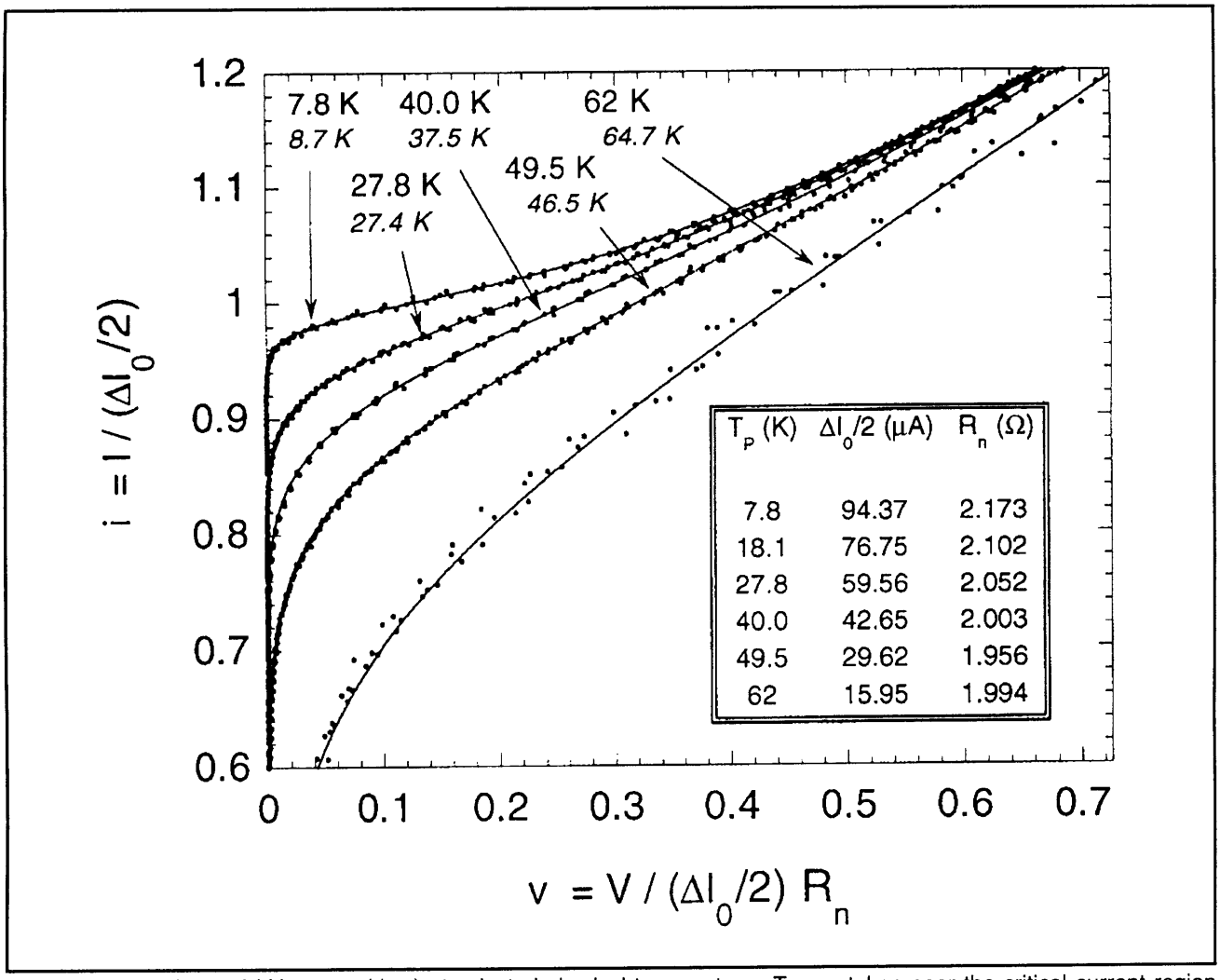

Figure 7. Experimental I-V curves (dots) at selected physical temperatures Tp are taken near the critical current region and fitted with I-V curves calculated from Eqs. (1)-(3) (solid lines). The simulated noise temperature T_N is in italics and the physical temperature is in normal text. The current and voltage scales are normalized, and the scaling parameters used are found in the inset.

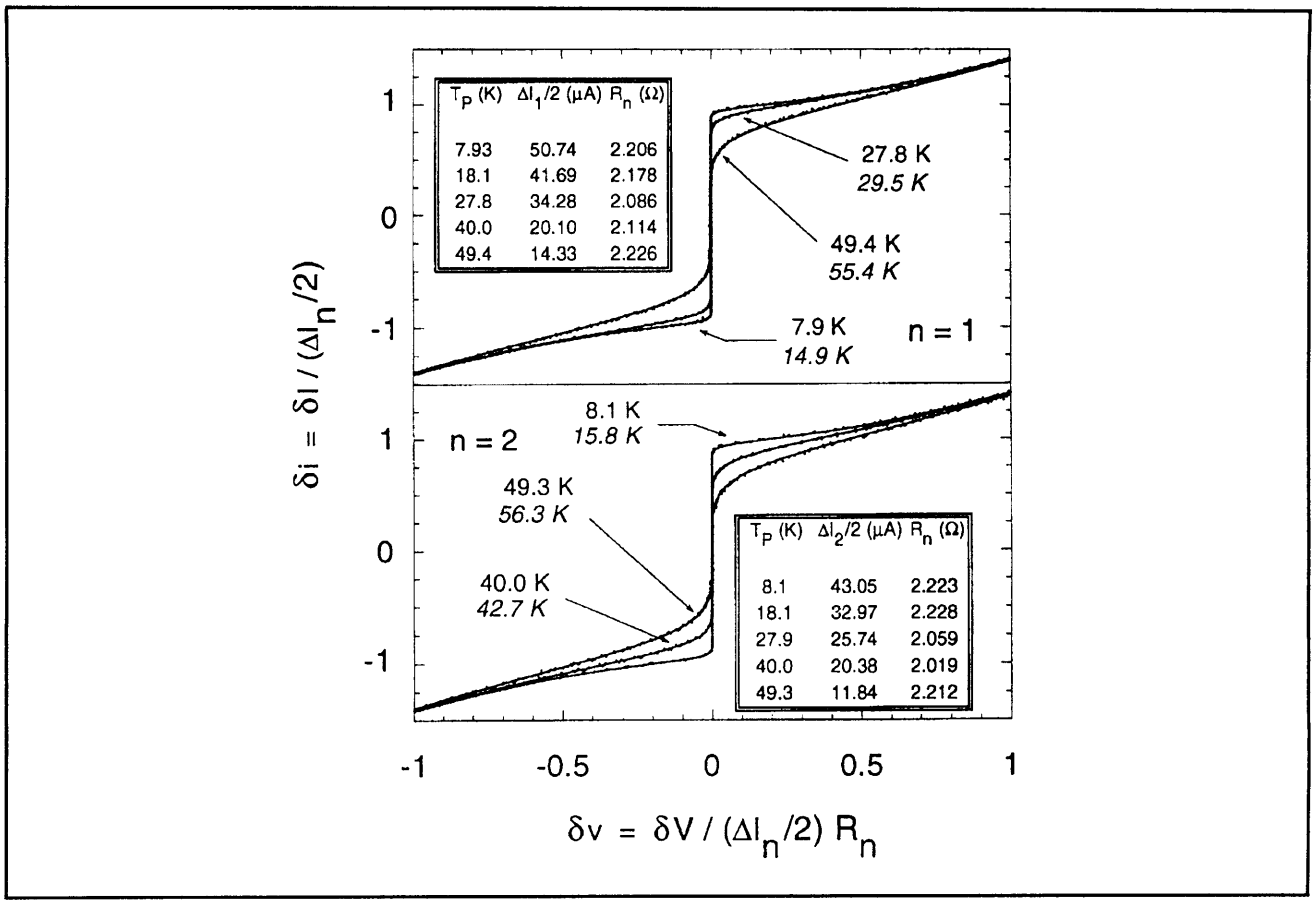

Figure 8. Similar to figure 7, the first and second Shapiro steps under 176 GHz coherent radiation are plotted against theoretical noise-rounded I-V curves.

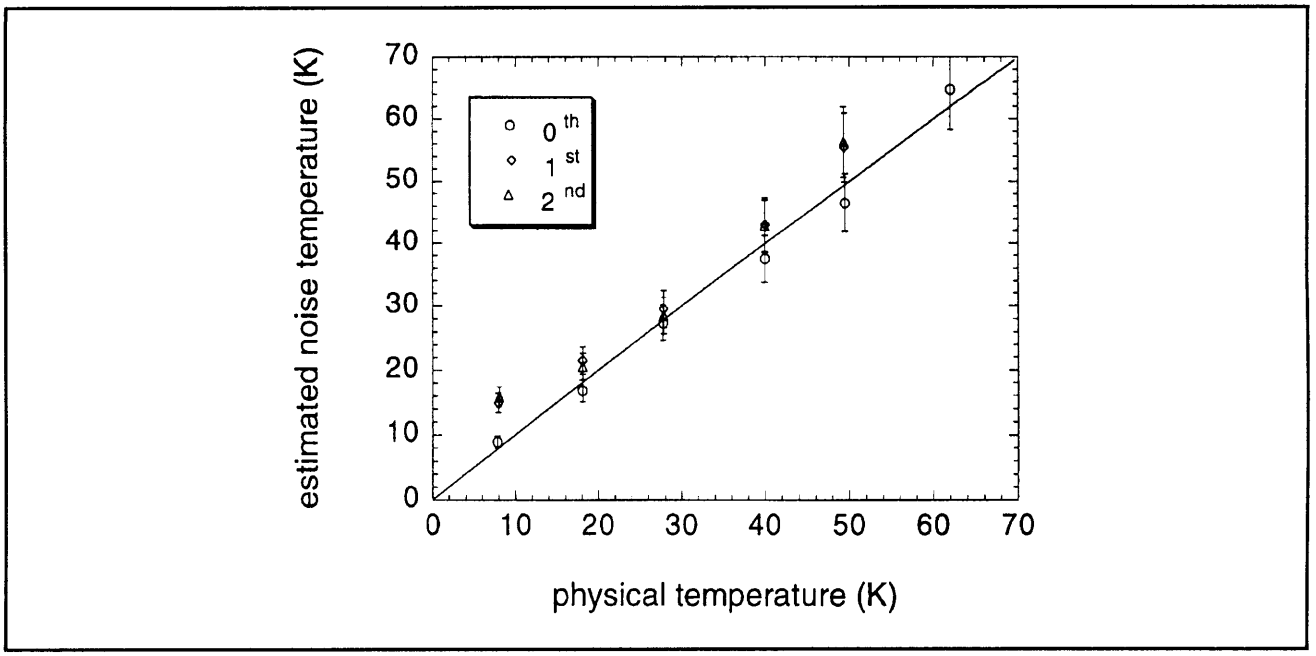

Figure 9. Estimated noise temperature at the zeroth, first, and second steps are plotted versus physical temperature. Error bars result from possible errors in the measurement apparatus and do not represent inconsistencies of fitting data. The dashed line of slope 1 gives $T_N = T_p$.

3.5 Millimeter-wave and Infrared Superconducting Focal-plane Receiver Arrays

Sponsors

MIT Lincoln Laboratory
National Aeronautics and Space Administration
Grant NAG2-693

Project Staff

Brian R. Jacobson, Professor Qing Hu, in collaboration with MIT Lincoln Laboratory

Millimeter wave and far-infrared frequencies remain one of the most underdeveloped frequency ranges, even though the potential applications in remote sensing and communication are obviously great. This is because the millimeter wave and far-infrared frequency range falls between two other frequency ranges in which conventional semiconductor devices are usually operated. One is the microwave frequency range, and the other is the near-infrared and optical frequency range. Semiconductor devices which utilize the classical diffusive transport of electrons, such as diodes and transistors, have a high frequency limit. This limit is set by the time it takes electrons to travel a certain distance. Currently, electron mobility and the smallest feature size which can be fabricated by lithography limit the frequency range to below 100 GHz. This limit probably cannot be pushed much higher. Semiconductor devices based on quantum mechanical interband transitions, however, are limited to frequencies higher than those corresponding to the semiconductor energy gap, which is higher than 10 THz for most bulk semiconductors. Therefore, a huge gap exists from 100 GHz to 10 THz in which very few devices are available.

The gap energies of conventional superconductors, such as Nb, are in the range of 100 GHz to 2 THz. This coincidence makes superconducting devices natural candidates for millimeter and submillimeter wave applications. At millimeter wave frequencies, the superconducting video detectors have been demonstrated to have quantum efficiency $e/\hbar\omega$; that is, a transport of one electron for one incoming photon; while the superconducting coherent receivers have been demonstrated to have their sensitivities limited only by the zero-point fluctuation of vacuum. Such receivers have been used widely in astrophysical studies. More applications are feasible in space-based communication and far-infrared spectroscopy which requires the ultimate sensitivity.

We are currently developing a novel scheme to couple the millimeter-wave and infrared signals to the superconducting devices by using a micromachined horn antenna and a planar antenna supported by a thin ($\sim 1\mu$m) membrane, as shown in figure 10. This scheme combines the advantages of easy fabrication of lithographic thin-film structures and the high antenna efficiencies of horn antennas. Because of the absence of substrate losses in this scheme, it is expected that a THz receiver can be constructed using all-Nb superconductor-insulator-superconductor (SIS) junctions. More important, because of the cumbersome mechanical structures used in conventional waveguide technology, microwave receivers have been single-element devices, as opposed to CCD imaging arrays at optical frequencies. Spatial scan has been achieved mechanically. Using the novel quasioptical scheme mentioned above, focal-plane detector arrays can be fabricated lithographically on a single Si wafer, as shown in figure 11, and far-infrared imaging becomes feasible.

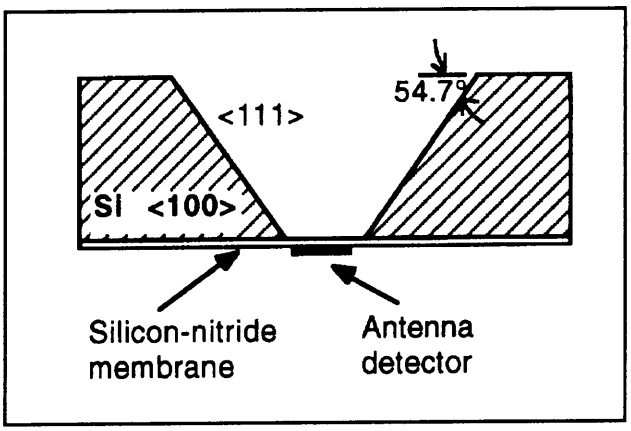

Figure 10. Example of anisotropic etching in a <100> silicon wafer. The opening of the wafer yields a pyramidal horn with a flare angle of 35.5 degrees.

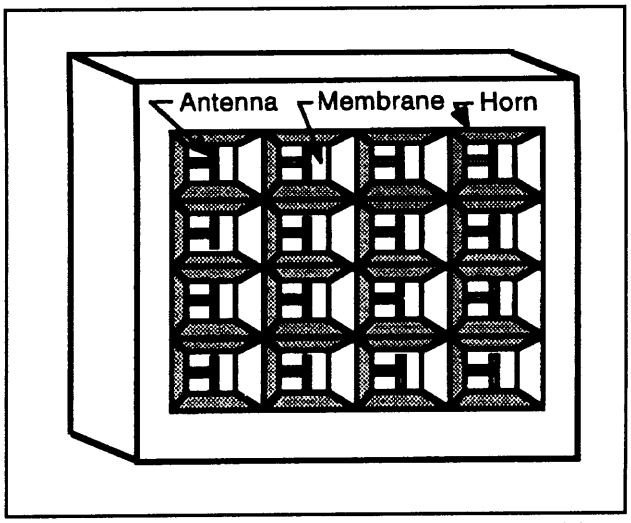

Figure 11. Perspective view of a two-dimensional horn imaging array.

The first step of this project is to demonstrate the feasibility of fabricating high-quality SIS devices on free-standing SiN membranes, and to demonstrate that these devices can survive thermal cycling. Using the microfabrication facilities in Group 86 at MIT Lincoln Laboratory, we have fabricated several wafers of SIS junctions with a critical current density of 4-6 kA/cm_2. We then etched the underneath Si wafer anisotropically in a KOH solution. A picture of an SIS junction with a dipole antenna on a 1-μm thick SiN membrane is shown in figure 12. Extreme care was taken to protect the SIS junctions from the KOH etchant during the anisotropic etching. Figure 13 shows the I-V curves of the SIS junction measured before and after the Si wafer was etched away. There are no noticeable changes in the I-V characteristics of the device. Clearly, our work has established the feasibility of building millimeter-wave SIS receivers using micromachined horn antenna structures. The referee of our paper,[4] which was recently published in *Applied Physics Letters*, commended this work in his remark, "Very important work—This is the next generation of millimeter and submillimeter astronomical receivers. Publish!"

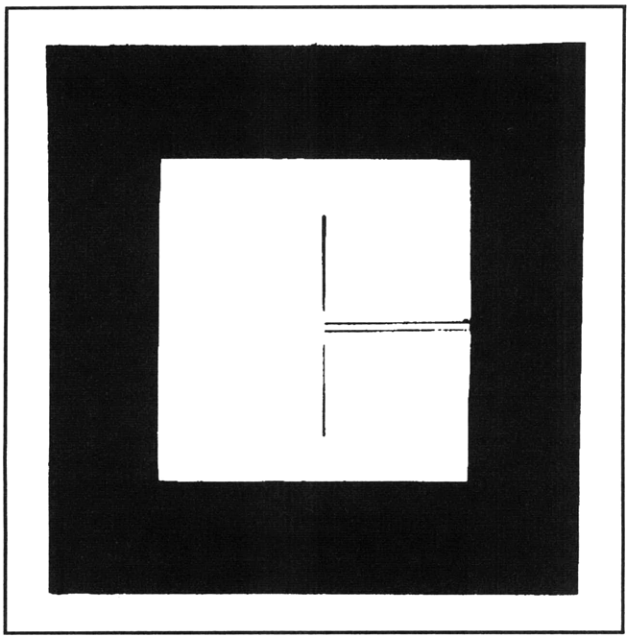

Figure 12. Photograph of an SIS device with a dipole antenna and a micromachined horn structure. View of the device seen through the membrane using back illumination of a microscope.

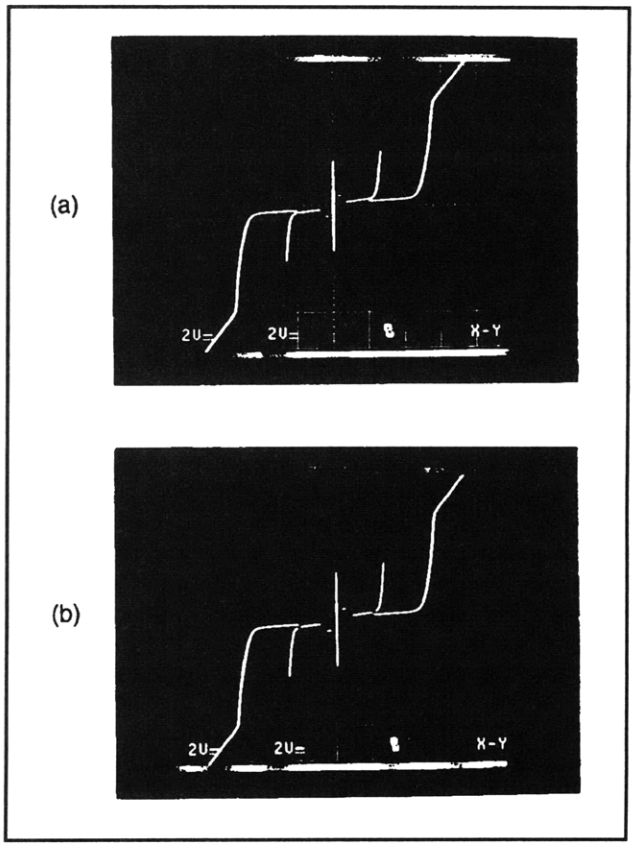

Figure 13. DC I-V curves for a device on SiN membrane (a) before etching, and (b) after etching the Si wafer in KOH.

3.6 Far-infrared (THz) Lasers Using Multiple Quantum Wells

Sponsor

U.S. Army Research Office
Grant DAAL03-92-G-0251

Project Staff

James Ernstmeyer, Jurgen H. Smet, Professor Qing Hu, in collaboration with Professor Clifton G. Fonstad, Jr.

Semiconductor quantum wells are man-made quantum mechanical systems in which the energy levels can be chosen by changing the sizes of the quantum wells. Typically, the frequency corresponding to the intersubband transitions is in the far-infrared or THz range. Naturally, long-wavelength photoelectric devices, such as far-

[4] E. Garcia, B.R. Jacobson, and Q. Hu, "Fabrication of High-quality SIS Junctions on Thin SiN Membranes," *Appl. Phys. Lett.* 63: 1002 (1993).

infrared lasers, which utilize the intersubband transitions have been proposed and subsequently studied. Significant progress has been made recently toward this goal. Large oscillator strengths of intersubband transitions have been observed in far-infrared absorption spectroscopy experiments. An intersubband spontaneous emission with a power level of $\sim 10^{-7}$ W has been observed. Although these preliminary results are encouraging, two major challenges to building a quantum-well far-infrared laser still remain. One is to achieve a high degree of population inversion between two subband levels, and the other is the confinement of photons within the active region. Optical pumping has low efficiency and low modulation speed; thus it would be difficult to achieve sufficient gain to maintain lasing oscillation and would be unsuitable for communication applications. As far as optical confinement is concerned, the usual dielectric waveguide confinement method, commonly used in optical and near-infrared laser systems, is not application at far-infrared frequencies because the confinement (on the order of a wavelength) is too large compared to the dimensions of the active region.

In this project, we will use a novel multiple quantum-well (MQW) device to circumvent these two problems. In this device, whose energy band diagram is shown in figure 14 with and without a dc bias voltage, electrons are injected selectively into an upper subband level of a wide lasing quantum well through a narrow filter quantum well. After relaxing into a lower subband in the lasing well, the electrons are then removed selectively to a collector through another narrow filter quantum well. This filter well prevents the electrons in the upper subband level from tunneling out to the collector. Using this method of selective injection and removal, a high degree of population inversion can be achieved, provided the tunneling rate of the electrons from the ground state to the collector is greater than the relaxation rate of the electrons from the upper subband to the ground state. Our calculation indicates that this should be achieved easily.

In the proposed MQW laser device, a parallel-plate waveguide that confines the photons can be formed between a heavily doped semiconductor injector and collector. At a doping level of $2 \times 10^{18}/cm^3$, we can raise the plasma frequency in the injector and collector to about 17 THz. It has been reported that the electron mobility, μ, for such a high doping level is 5×10^3 cm^2/Vs. This plasma is mostly reflective with a penetration depth as short as 0.8 μm for a lasing frequency in the range of 1-8 THz. This confinement is sufficiently tight so that the lasing threshold current density is on the order of several hundred A/cm^2, which should be achievable.

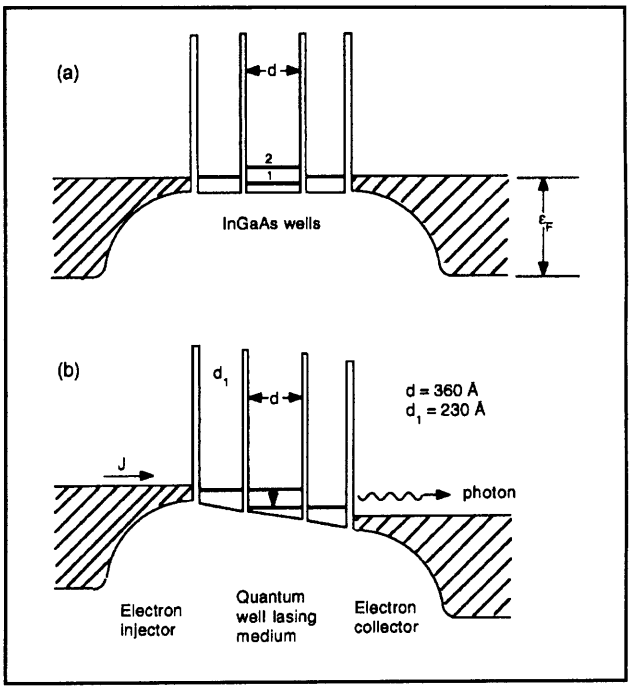

Figure 14. Band profiles (not drawn in proportion) of the proposed far-infrared laser device under (a) zero-bias, and (b) lasing condition in which $V_{bias} \sim (E_2 - E_1)/e \approx 20$mV. The device consists of one narrow quantum-well energy filter on both sides of the lasing quantum well. The width of the narrow filter wells (made of $In_{0.53}Ga_{0.47}As$) is approximately 230 Å, so the energy of its first subband lies in between the first two subbands in the wide lasing well whose width is approximately 360 Å, which will have a radiation frequency of 5 THz due to the intersubband transitions.

The first step of this project is to fabricate multiple quantum-well structures with different well widths and barrier thicknesses, and to perform tunneling spectroscopy on them to determine the relative positions of the subbands in different quantum wells. Because of the small energy differences which are associated with the relatively wide quantum wells, the tunneling spectroscopy must be performed at liquid helium temperatures. Our initial measurements on the tunneling I-V characteristics revealed many features which could be attributed to elastic tunneling and LO phonon-assisted inelastic tunneling.

To interpret the fine features of the I-V characteristics with greater certainty, we have employed a powerful method, *magnetotunneling spectroscopy,* to study the relative positions of the subbands under concern. In addition to spectroscopy, this study has a practical purpose for laser applications. The nonradiative intersubband relaxation rate due to phonon emissions is much greater than that of the radiative relaxation rate. This is mainly because the transverse motion of electrons in the lasing quantum well is unrestricted, so there is a

large volume in the phase space into which the electrons are scattered. Similar to the concept employed in a tokamak to confine plasmas, a strong magnetic field will restrict the electron motions in the transverse directions. This magnetic field-induced transverse confinement, along with the longitudinal confinement provided by the quantum well, will effectively reduce the dimensionality of the electron system to that of a zero-dimensional system, just like that of quantum dot systems. Therefore, the nonradiative relaxation rate can be substantially reduced. Because the magnetic field does not affect the longitudinal motion of electrons, electrical pumping is still possible which is difficult to implement for quantum dot systems which are formed geometrically.

We have performed magnetotunneling spectroscopy on a double quantum-well structure which consists of 115-Å and 200-Å $In_{0.53}Ga_{0.47}As$ quantum wells, both are confined by 30 Å of $In_{0.52}Al_{0.48}As$ respectively on the top and bottom and separated by a 60-Å $In_{0.52}Al_{0.48}As$ middle barrier. When a longitudinal magnetic field is applied, the tunneling current is modulated by the field, as shown in Figure 15a. The magneto-oscillation is periodic with the inverse of the magnetic field 1/B. Thus, a Fourier transform of this magneto-oscillation in 1/B gives a peak which centers at a characteristic field B_o, as shown in figure 15b.

The physical origin of this magneto-oscillation is scattering-mediated inter-Landau level tunneling. Suppose the energy in the first well is given by $E_1 + (n_1 + 1/2)\hbar eB/m^*$, and the energy in the second well is $E_2 + (n_2 + 1/2)\hbar eB/m^*$, where E_1 and E_2 are the energies of the subbands in the first and second well under concern. In the absence of LO phonon emissions, energy conservation requires the two energies to be equal. Thus, $(n_2 - n_1)\hbar eB/m^* = E_1 - E_2$, or $1/B = (n_2 - n_1)\hbar e/m^*(E_1 - E_2)$. This implies that whenever 1/B is an integer times the inverse of a characteristic field $1/B_o = \hbar e/m^*(E_1 - E_2)$, the energy conservation is satisfied and the tunneling current will be enhanced, which gives the oscillatory behavior of the tunneling current as a function of 1/B, as shown in Figure 15a.

Since the energy difference between the two subbands is related to B_o through $E_1 - E_2 = \hbar eB_o/m^*$, this magnetotunneling spectroscopy provides us with a very accurate method to measure the relative positions of the subbands under concern. Figures 16 and 17 show the subband energy levels as functions of bias voltage in both forward and reversed polarities. These measured energy levels are within 5 percent from the designed values, which is remarkable considering the relatively small energy scales (~ 10 meV) for far-infrared applications. This accurate determination of subband energy levels is crucial in successfully developing far-infrared sources with specific frequencies.

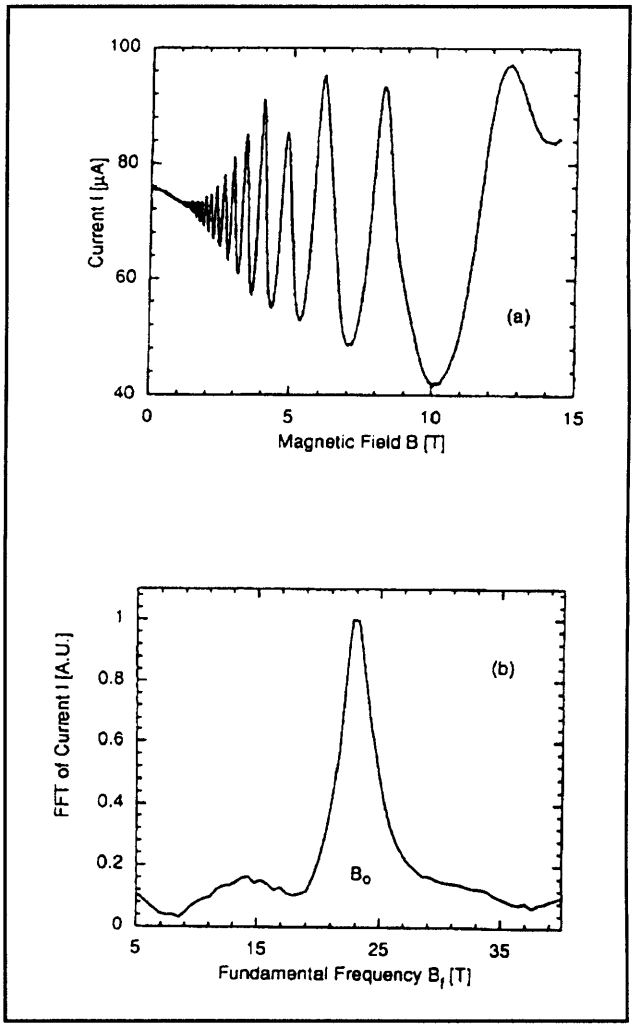

Figure 15. (a) Tunneling current (at a fixed bias voltage) as a function of the strength of a magnetic field applied in the same direction as that of the tunneling current. (b) Fourier transform of the tunneling current as a function of 1/B.

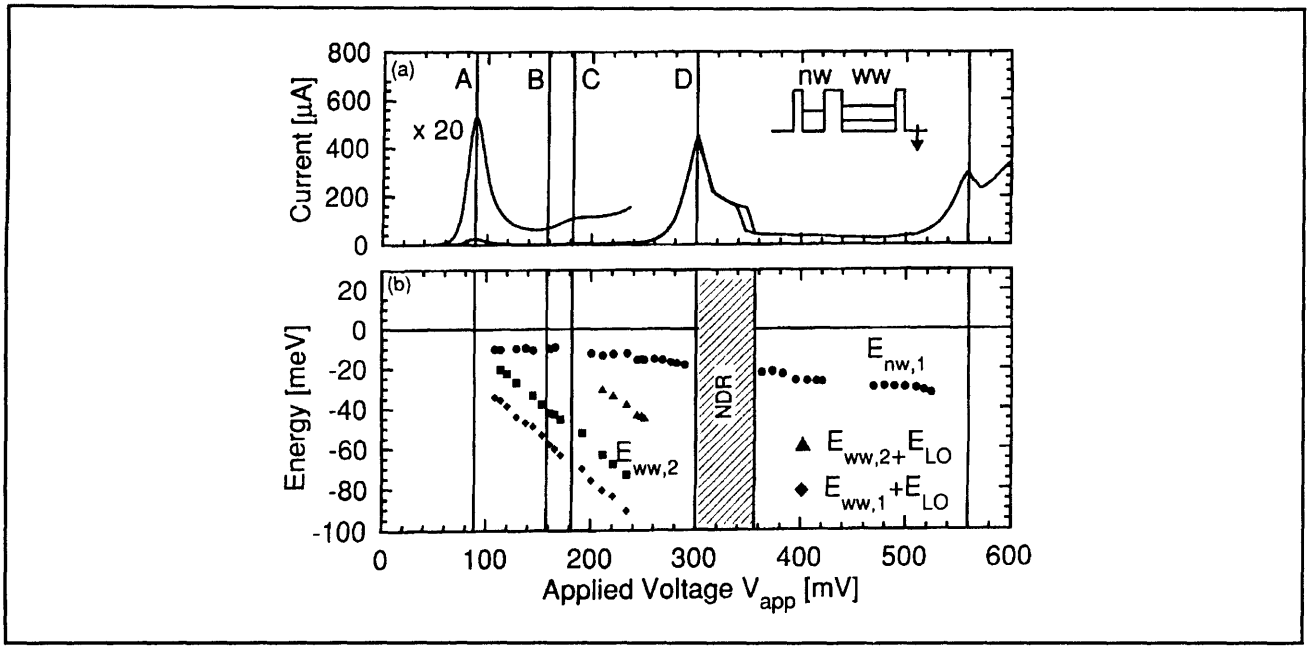

Figure 16. The I-V characteristic (a) and the subband energies (b) as a function of applied forward bias at 4.2 K. The quasi-Fermi level in the emitter well is used as the energy reference. Features A, B, C, and D are unambiguously identified as A: $E_{nw,1} \rightarrow E_{ww,2}$; B: onset of LO-phonon emission process $E_{nw,1} \rightarrow E_{ww,2} + E_{LO}$; C: all electrons in subband $E_{nw,1}$ can participate in LO-phonon emission process $E_{nw,1} \rightarrow E_{ww,2} + E_{LO}$; and D: $E_{nw,1} \rightarrow E_{ww,3}$. The measured (designed) intersubband energies are $E_{ww,2} - E_{ww,1} = 47$ (48) meV, and $E_{nw,2} - E_{nw,1} = 113$ (109) meV.

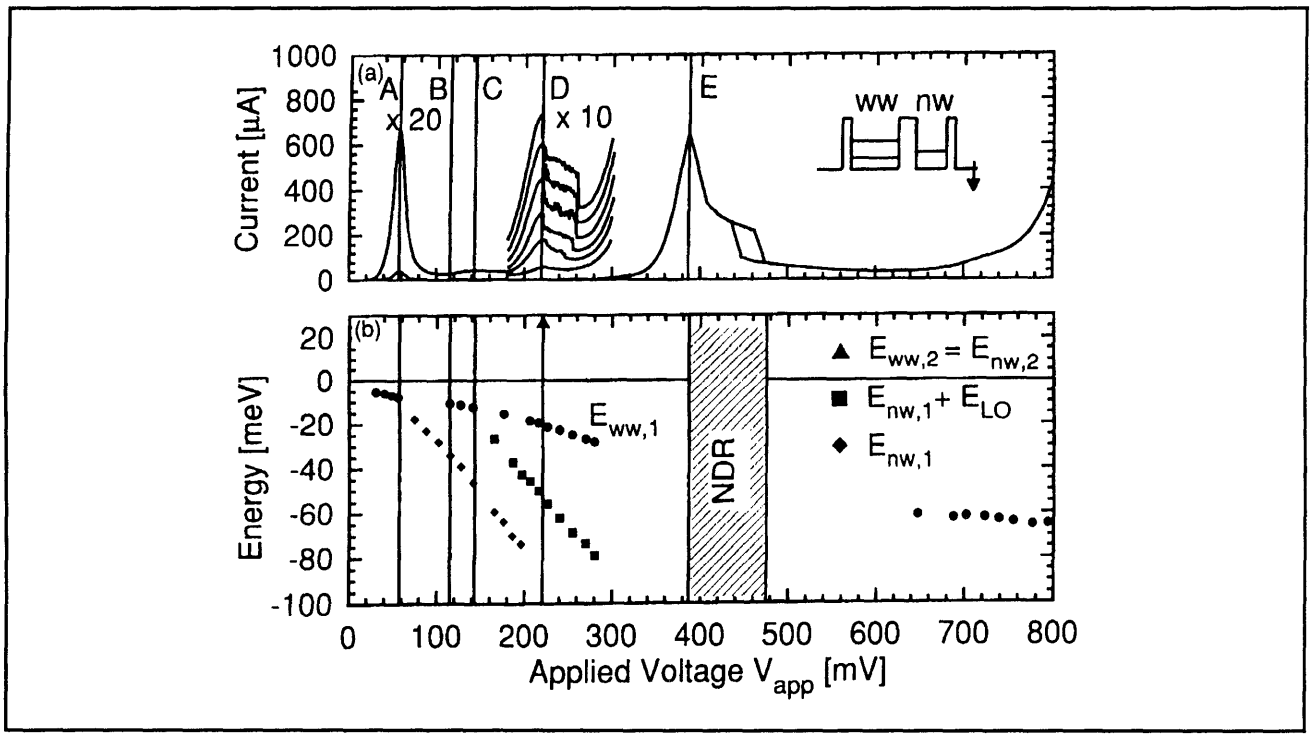

Figure 17. The I-V characteristic (a) and the subband energies (b) as a function of the applied reverse bias at 4.2 K. The quasi-Fermi level in the emitter well is used as the energy reference. Features A, B, C, D, and E are identified as A: $E_{ww,1} \rightarrow E_{nw,1}$; B: onset of LO-phonon emission process $E_{ww,1} \rightarrow E_{nw,1} + E_{LO}$; C: all electrons in subband $E_{ww,1}$ can participate in LO-phonon emission process $E_{ww,1} \rightarrow E_{nw,1} + E_{LO}$; D: $E_{ww,2} \rightarrow E_{nw,2}$; and E: $E_{ww,1} \rightarrow E_{nw,2}$. The measured (designed) intersubband energies are $E_{ww,2} - E_{ww,1} = 52$ (48) meV, and $E_{ww,3} - E_{ww,2} = 76$ (70) meV.

3.7 Publications

Feng, S., and Q. Hu. "Far-infrared Photon-assisted Transport through Quantum Point Contact Devices." *Phys. Rev. B* 48: 5354 (1993).

Garcia, E., B.R. Jacobson, and Q. Hu. "Fabrication of High-quality SIS Junctions on Thin SiN Membranes." *Appl. Phys. Lett.* 63: 1002 (1993).

Gupta, R., Q. Hu, D. Terpstra, G.J. Gerritsma, and H. Rogalla. "Near-millimeter-wave Response of High-Tc Ramp-Type Josephson Junctions." *Appl. Phys. Lett.* 62: 3351 (1993).

Gupta, R., Q. Hu, D. Terpstra, G.J. Gerritsma, and H. Rogalla. "A Noise Study of a High-Tc Josephson Junction under Near-millimeter-wave Irradiation." *Appl. Phys. Lett.* 64: 927 (1994).

Hu, Q. "Photon-assisted Quantum Transport in Quantum Point Contacts." *Appl. Phys. Lett.* 62: 837 (1993).

Smet, J.H., C.G. Fonstad, and Q. Hu. "Magneto-tunneling Spectroscopy in Wide $In_{0.53}Ga_{0.47}As/In_{0.52}Al_{0.48}As$ Double Quantum Wells." *Appl. Phys. Lett.* 63: 2225 (1993).

Wyss, R.A., C.C. Eugster, J.A. del Alamo, and Q. Hu. "Far-infrared Photon-induced Current in a Quantum Point Contact." *Appl. Phys. Lett.* 63: 1522 (1993).

3.7.1 Meeting Papers

Gupta, R., Q. Hu, D. Terpstra, G.J. Gerritsma, and H. Rogalla. "The Response of YBCO/PBCO/YBCO Ramp Type Junctions to Near-millimeter-wave Radiation." Paper presented at the 1993 APS March meeting, Seattle, Washington; *Bull. Amer. Phys. Soc.* 38: 637 (1993).

Hu, Q., R.A. Wyss, C.C. Eugster, J.A. del Alamo, S. Feng, M.J. Rooks, and M.R. Melloch. "A Novel Submillimeter-wave Detector Using Quantum Point Contacts." *Proceedings of the Fourth International THz Conference* 605 (1993).

Hu, Q., R. Gupta, D. Terpstra, G.J. Gerritsma, and H. Rogalla. "Response of Ramp-Type High-Tc Josephson Junctions to Near Millimter-wave Radiation." *Proceedings of the Fourth International THz Conference* 539 (1993).

Hu, Q., J.H. Smet, and C.G. Fonstad. "Terahertz Lasers Using Quantum-well Structures." Paper presented at the SPIE International Symposium (OE/LASE '94), Los Angeles, California, January 25, 1994.

Hu, Q., R. Gupta, D. Terpstra, G.J. Gerritsma, and H. Rogalla. "Response of High-Tc Ramp-type Josephson Junctions to Near-millimeter-wave Radiation." Paper presented at the SPIE International Symposium (OE/LASE '94), Los Angeles, California, January 26, 1994.

Hu, Q., R.A. Wyss, C.C. Eugster, J.A. del Alamo, and S. Feng. "Far-infrared Study of an Antenna-coupled Quantum Point Contact." Paper presented at the NATO Advanced Research Workshop on Quantum Well Intersubband Transition Physics and Devices, Whistler, Canada, September 8, 1993. Forthcoming.

Hu, Q., R. Gupta, D. Terpstra, G. J. Gerritsma, and H. Rogalla. "Millimeter-wave Studies of High-Tc Ramp-Type Josephson Junctions." Paper presented at 1993 International Semiconductor Device Research Symposium (ISDRS), Charlottesville, North Carolina, December 2, 1993; *ISDRS Proc.* 483 (1993).

Smet, J.H., C.G. Fonstad, and Q. Hu. "Magneto-tunneling spectroscopy in Wide $In_{0.53}Ga_{0.47}As/In_{0.52}Al_{0.48}As$ Double Quantum Wells." Paper presented at the 1993 APS March meeting, Seattle., Washington, 1993; *Bull. Amer. Phys. Soc.* 38: 813 (1993).

Wyss, R.A., C.C. Eugster, J. del Alamo, M.J. Rooks, M.R. Melloch, and Q. Hu. "Far-infrared Study of an Antenna-coupled Quantum Point Contact." Paper presented at 1993 International Semiconductor Device Research Symposium (ISDRS), Charlottesville, December 2, 1993; *ISDRS Proc.* 667 (1993).

Theses

Gupta, R.K. *Near-millimeter-wave Response and Noise in High-Tc Ramp-type Josephson Junctions.* S.M. thesis. Dept. of Electr. Eng. and Comput. Sci., MIT, May 1993.

Jacobson, B.R. *Micromachined Millimeter-wave SIS Receivers.* S.M. thesis. Dept. of Electr. Eng. and Comput. Sci., MIT, May 1994.